ACADEMIC PRESS

Available online at www.sciencedirect.com

SCIENCE DIRECT®

Journal of Magnetic Resonance 158 (2002) 173–177

JMR Journal of Magnetic Resonance

www.academicpress.com

Communication

Sensitivity-enhanced E.COSY-type HSQC experiments for accurate measurements of one-bond ^{15}N–$^{1}H^{N}$ and ^{15}N–$^{13}C'$ and two-bond $^{13}C'$–$^{1}H^{N}$ residual dipolar couplings in proteins

Keyang Ding and Angela M. Gronenborn*

Laboratory of Chemical Physics, National Institute of Diabetes and Digestive and Kidney Diseases, National Institutes of Health, Bethesda, MD 20892, USA

Received 5 June 2002; revised 31 July 2002

Abstract

Novel E.COSY-type HSQC experiments are presented for the accurate measurement of one-bond ^{15}N–$^{1}H^{N}$ and ^{15}N–$^{13}C'$ and two-bond $^{13}C'$–$^{1}H^{N}$ residual dipolar couplings in proteins. Compared with existing experiments, the (δ, J)-E.COSY experiments described here are composed of fewer pulses and the resulting spectra exhibit 1.4 times the sensitivity of coupled HSQC spectra. Since residual dipolar couplings play increasingly important roles in structural NMR, the proposed methods should find wide spread application for structure determination of proteins and other biological macromolecules.

Keywords: Residual dipolar couplings; E.COSY; Proteins; Structural genomics

The importance of residual dipolar couplings has been amply documented for protein structure determination by NMR spectroscopy [1–3]. Five different kinds of couplings are commonly employed, namely, one-bond ^{15}N–$^{1}H^{N}$, ^{15}N–$^{13}C'$, $^{13}C'$–$^{13}C^{\alpha}$, $^{13}C^{\alpha}$–$^{1}H^{\alpha}$, and two-bond $^{13}C'$–$^{1}H^{N}$ couplings along the polypeptide backbone [3]. In general, residual dipolar couplings can simply be obtained from the difference in J couplings measured in the presence of an alignment medium [4–6] and in isotropic solution, given that the observed J is the sum of scalar and dipolar coupling. Residual dipolar couplings provide a set of long-range constraints that allow further refinement of traditional protein NMR structures or aid in the determination of domain orientation in multi-domain proteins. Therefore, accurate and efficient methods for extracting these couplings are of major importance in structural NMR. Here, we describe novel, sensitivity-enhanced E.COSY type HSQC experiments that can be used for this purpose. In particular, we present pulse sequences for measuring one-bond ^{15}N–$^{1}H^{N}$ and ^{15}N–$^{13}C'$ and two-bond $^{13}C'$–$^{1}H^{N}$ couplings in proteins.

One-bond ^{15}N–$^{1}H^{N}$ dipolar couplings are routinely determined from coupled HSQC spectra in a simple and efficient manner. Drawbacks of coupled HSQC experiments are their relatively low sensitivity, just half of that of in a decoupled HSQC spectrum. In addition, overlap problems due to coupled pairs are encountered and it frequently becomes difficult to unambiguously assign the individual partners of the pairs in crowded spectral regions. Although there are a number of experiments [7–9] for accurate measurements of one-bond ^{15}N–$^{1}H^{N}$ couplings, a frequently employed method uses the IPAP approach [10]. One-bond ^{15}N–$^{13}C'$ couplings can also be extracted from so-called quantitative J-correlation experiments [11] using intensity analysis [12]. The accuracy of the intensity analysis, however, is critically determined by the signal-to-noise ratio in the spectra. Another way to measure one-bond ^{15}N–$^{13}C'$ couplings and the only way to determine the two-bond $^{13}C'$–$^{1}H^{N}$ couplings consists of separating the two $^{13}C'$–$^{1}H^{N}$ doublet components in the HSQC spectra based on the E.COSY principle [13]. Unfortunately, the resulting

* Corresponding author. Fax: 1-301-496-1690.
E-mail address: gronenborn@nih.gov (A.M. Gronenborn).

1090-7807/02/$ - see front matter © 2002 Elsevier Science (USA). All rights reserved.
PII: S1090-7807(02)00024-1

HSQC spectrum with E.COSY splittings [14] from passive $^{13}C'$-nuclei has only low resolution and low sensitivity. Compared to ^{15}N–$^{1}H^{N}$ dipolar couplings, $^{13}C'$–$^{1}H^{N}$, and ^{15}N–$^{13}C'$ couplings are approximately three and eight times smaller due to the longer internuclear distance and the gyromagnetic ratios involved. Such small couplings are clearly more difficult to measure accurately and reliably. In particular, any overlap between components of the E.COSY pairs will have detrimental effects on the accuracy of the extracted coupling, given that the position of the peak maximum is affected by the overlap [15]. For any splitting that is measured from the relative peak displacement, one has to keep in mind that the accuracy of the peak position is directly proportional to the signal-to-noise ratio and is inversely related to the line width, thereby limiting the attainable accuracy considerably. In addition, problems caused by overlap or imperfect phasing can never be completely avoided.

The pulse sequences of the proposed sensitivity-enhanced E.COSY-type HSQC experiments are illustrated in Fig. 1. The sequence displayed in (a) is used to measure the one-bond ^{15}N–$^{1}H^{N}$ coupling and is easily understood using the product operator formalism [16]. The magnetization at the beginning of the evolution period t_1 is described by $\sigma(0) = -2H_zN_y$, where H and N represent the proton and nitrogen magnetizations, respectively. This magnetization evolves under the ^{15}N chemical shift frequency ω_N and becomes $\sigma(t_1)$ at the end of the evolution period

$$\sigma(t_1) = -2H_zN_y\cos(\omega_N t_1) + 2H_zN_x\sin(\omega_N t_1). \quad (1)$$

The mixing pulses simultaneously transform $2H_zN_y$ into $-H_x$ and $2H_zN_x$ into $-2H_yN_z$. At the beginning of the detection period t_2, the magnetization $\sigma(t_1, 0)$ can be described by

$$\sigma(t_1, 0) = H_x\cos(\omega_N t_1) - 2H_yN_z\sin(\omega_N t_1). \quad (2)$$

As evidenced by Eq. (2), the phase after evolution of the ^{15}N chemical shift frequency ω_N during the t_1 period becomes the initial phase of the ^{15}N–$^{1}H^{N}$ coupling evolution during the t_2 period. During the detection period, the detectable magnetization can be expressed as

$$\begin{aligned}\sigma(t_1, t_2) &= H_x\cos(\omega_H t_2)\cos(\pi J_{NH} t_2 + \omega_N t_1) \\ &\quad + H_y\sin(\omega_H t_2)\cos(\pi J_{NH} t_2 + \omega_N t_1) \\ &= H_x[\cos(\omega_H t_2 + \pi J_{NH} t_2 + \omega_N t_1) \\ &\quad + \cos(\omega_H t_2 - \pi J_{NH} t_2 - \omega_N t_1)]/2 \\ &\quad + H_y[\sin(\omega_H t_2 + \pi J_{NH} t_2 + \omega_N t_1) \\ &\quad + \sin(\omega_H t_2 - \pi J_{NH} t_2 - \omega_N t_1)]/2. \end{aligned} \quad (3)$$

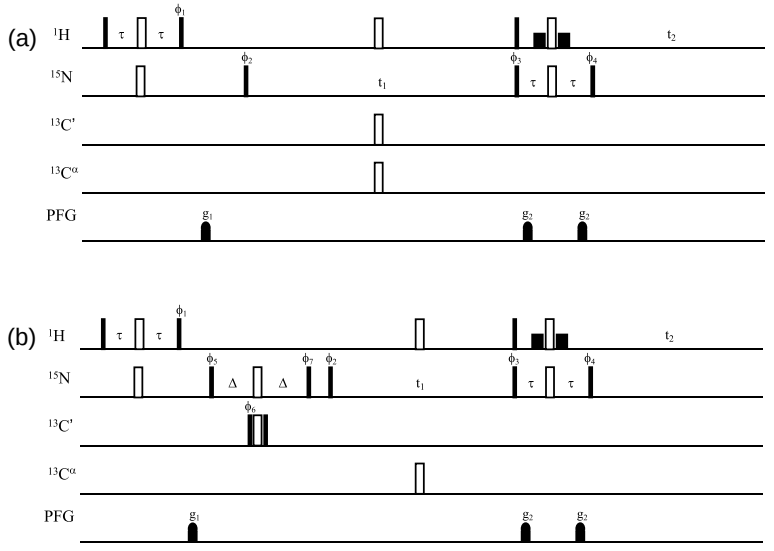

Fig. 1. Pulse sequences of sensitivity-enhanced (δ, J)-E.COSY HSQC experiments for measuring one-bond ^{15}N–$^{1}H^{N}$ and ^{15}N–$^{13}C'$ and two-bond $^{13}C'$–$^{1}H^{N}$ couplings. Narrow (filled) and wide (open) bars represent 90° and 180° pulses with phase x, respectively, unless indicated elsewhere. Proton 90° soft pulses with 1 ms duration are used for Watergate and they are indicated by short-filled bars. The carrier frequencies in the ^{1}H, ^{15}N, $^{13}C'$, and $^{13}C^{\alpha}$ channels are positioned at 4.7 (water resonance), 118, 177, and 56 ppm, respectively. The power level for $^{13}C'$ and $^{13}C^{\alpha}$ pulses is set at $\Delta\omega_0/(3)^{1/2}$, where $\Delta\omega_0$ is the difference in Hz between $^{13}C'$ and $^{13}C^{\alpha}$ carrier frequencies. The inter-pulse delays are $\tau = 2.5$ ms and $\Delta = 17.5$ ms. The PFG g_1 and g_2 are sine-shaped with maximal 20 G/cm with durations of 3 and 0.6 ms, respectively. The phase ϕ_2 is incremented by 90° synchronously with incrementing t_1, which is incremented in States manner [24]. In (a), the phase cycles are as the follows: $\phi_1 = y,\ \phi_2 = x, -x,\ \phi_3 = x,x,-x,-x,\ \phi_4 = y,y,-y,-y$, and $\phi_{Rec} = x,-x,-x,x$, and the phase ϕ_4 is incremented by 180° to achieve acquisition of echo and anti-echo signals in the two successive experiments of the 2D series. In (b), the phase cycles for the in-phase data set are as follows: $\phi_1 = y$, $\phi_2 = x,\ \phi_3 = x,x,-x,-x,\ \phi_4 = y,y,-y,-y,\ \phi_5 = x,-x,\ \phi_6 = x,\ \phi_7 = x,x,x,x,-x,-x,-x,-x$, and $\phi_{Rec} = x,-x,-x,x,-x,x,x,-x$, and the phase cycles for anti-phase dataset are: $\phi_1 = y,\ \phi_2 = x,\ \phi_3 = x,x,-x,-x,\ \phi_4 = y,y,-y,-y,\ \phi_5 = x,-x,\ \phi_6 = -x,\ \phi_7 = y,y,y,y,-y,-y,-y,-y$, and $\phi_{Rec} = x,-x,-x,x,-x,x,x,-x$. Adding or subtracting the in-phase and anti-phase data sets yields two new data sets which are Fourier transformed. The phase ϕ_4 is incremented by 180° to achieve acquisition of echo and anti-echo signals in the two successive experiments of the 2D series.

In Eq. (3), the first and third terms describe the real and imaginary parts of the low field (high frequency) peak of the $^1J_{NH}$ doublet that belongs to the nitrogen with frequency ω_N. The second and forth terms correspond to the real and imaginary parts of high field (low frequency) peak of the $^1J_{NH}$ doublet, belonging to the nitrogen with frequency $-\omega_N$. Therefore, an E.COSY-type cross peak [14] centered at $(0,\omega_H)$ is created exhibiting splittings of $2\omega_N$ and $^1J_{NH}$ along the ω_1 and ω_2 dimensions, respectively. Inverting the sign of the phase ϕ_4, the sign of second term in Eq. (2) is inverted correspondingly. This is equivalent to inverting the sign of ω_N. Therefore, Eq. (3) can be written as

$$\begin{aligned}\sigma(t_1,t_2) = {} & H_x[\cos(\omega_H t_2 + \pi J_{NH} t_2 - \omega_N t_1) \\ & + \cos(\omega_H t_2 - \pi J_{NH} t_2 + \omega_N t_1)]/2 \\ & + H_y[\sin(\omega_H t_2 + \pi J_{NH} t_2 - \omega_N t_1) \\ & + \sin(\omega_H t_2 - \pi J_{NH} t_2 + \omega_N t_1)]/2. \end{aligned} \quad (4)$$

For the pulse sequence in Fig. 1a, Eqs. (3) and (4) accurately describe the $(2n-1)$th and $(2n)$th FIDs acquired at a given t_1 in the 2D series, respectively. The signals described by Eqs. (3) and (4) are echo and anti-echo with respect to one other. By manipulating the time domain data set in the echo, anti-echo manner [17,18], 2D Fourier transformation leads to a sensitivity-enhanced spectrum. In contrast to the conventional E.COSY spectrum in which two passive couplings from a third nuclear spin within the correlated spin-pair are compared, the present E.COSY spectrum compares the active one-bond coupling $^1J_{NH}$ and one chemical shift (ω_N) within the correlated spin pair. For convenience, we name this type of E.COSY experiment (δ,J)-E.COSY. The implementation of the (δ,J)-E.COSY experiment is based on a similar strategy as described previously for reduced dimensionality triple resonance spectra [19]. The spectral width in the ω_1-dimension is set to twice the ^{15}N chemical shift frequency range and an artificial ^{15}N resonance offset is achieved by using TPPI [20,21]. In this manner, the two peaks of each E.COSY peak-pair can be located in distinctly different regions of the 2D plane.

A sensitivity enhancement by a factor of 1.4 can be achieved for the (δ,J)-E.COSY-type HSQC experiment, retaining identical resolution to the decoupled HSQC spectrum if the digital resolution is the same as in the coupled HSQC spectrum. This follows from a comparison of two 2D experiments with identical t_1(max) and total measuring times: the spectral widths are $(SW_1)\times(SW_2)$ and $(2SW_1)\times(SW_2)$, and the number of scans and time domain data points are $(2NS)\times(TD_1)$ and $(NS)\times(2TD_1)$, respectively. Without any manipulation of the time domain data, the same 2D Fourier transformation results in two 2D spectra having the identical digital resolution albeit with a slight increase in signal-to-noise ratio in the latter because of the increased spectral width [22]. If the time domain data of latter experiment is manipulated in an echo, anti-echo manner, the resulting 2D Fourier transformation yields an identical digital resolution 2D spectrum with 1.4 times improved signal-to-noise [17,18]. This is equivalent to 0.7 times the sensitivity of the decoupled HSQC spectra. For any practical application, however, it is not necessary to keep the same digital resolution as in the coupled or decoupled HSQC spectra and the sensitivity can be further increased if t_1(max) is reduced.

In our (δ,J)-E.COSY experiment, the $^1J_{NH}$ couplings are measured in the homo-nuclear dimension, rather than in the hetero-nuclear dimension. The latter is standard practice in most existing experiments [7–10]. For the $^1J_{NH}$ coupling itself, no difference between the two dimensions exists. The $^1J_{NH}$ splitting in the hetero-nuclear dimension, however, may be affected by proton exchange if the exchange rate approaches the $^1J_{NH}$ coupling constant. For proteins aligned in liquid crystal media, the resulting error may be considerable. For the $^1J_{NH}$ splitting in the homo-nuclear dimension, the line-shape of $^1J_{NH}$ doublet may be distorted by $^3J_{^1H^N-H^\alpha}$ effects from coupling, combined with the cross-correlated ^{15}N–^1H and $^1H^N$–$^1H^\alpha$ dipolar relaxation. Fortunately, the cross-correlated ^{15}N–^1H and $^1H^N$–$^1H^\alpha$ dipolar relaxation rates are small and do not distort the line-shape of the $^1J_{NH}$ doublet significantly.

As for any experiment that contains pulses during the evolution period for measuring J couplings, corrections have to be made to correct for the finite pulse widths [8,23]. This represents a drawback for the routine use of such an experiment. It is therefore highly desirable, to let the coupled spin-pairs evolve, without being disturbed by any pulses during the evolution period. In addition, it is well known that higher sensitivity goes hand-in-hand with fewer pulses in multiple-pulse experiments. In this respect, the proposed (δ,J)-E.COSY experiment exhibits superior features compared to many of the existing methods.

The pulse sequence displayed in (b) is a modification of that in (a). The refocusing pulse in the $^{13}C'$ channel is omitted with the net effect that each cross peak in the resulting (δ,J)-E.COSY spectrum is split further by the attached $^{13}C'$ spin. For a coupled NH spin-pair with a passive coupling to a third $^{13}C'$ spin, the E.COSY splitting of the NH spin-pair is achieved without any pulse disturbance during the evolution and detection periods. Philosophically similar to the IPAP experiment [10], the E.COSY splitting from the $^{13}C'$ spin can be manipulated in-phase, if the magnetization at the beginning of evolution period is $2H_zN_x$, or anti-phase, if the magnetization at the beginning of evolution period is $4H_zN_yC'_z$. The magnetization $4H_zN_yC'_z$ is obtained by implementing a $N \rightarrow C'$ INEPT transfer step before the evolution period as shown in Fig. 1b. $2H_zN_x$ magnetization is created right after the INEPT transfer from

proton to nitrogen. For relaxation compensation, a refocusing delay of the same length as the $N \rightarrow C'$ INEPT transfer step is implemented. Using the pulse sequence in 1(b), two (δ, J)-E.COSY sub-spectra are obtained with in-phase and anti-phase E.COSY splitting from the passive $^{13}C'$ spin. Adding or subtracting these in-phase and anti-phase spectra yields two (δ, J)-E.COSY type spectra, in which the peak–pair centers are located at $(0, \omega_H + {}^2J_{CH}/2)$ and at $(0, \omega_H - {}^2J_{CH}/2)$, and the splittings represent $(2\omega_N + {}^1J_{NC}, {}^1J_{NH})$ and $(2\omega_N - {}^1J_{NC}, {}^1J_{NH})$. The entire pulse sequence can be implemented in an interleaved manner to obtain the in-phase and anti-phase spectra. Alternatively, by combining two sets of phase cycling, these two spectra can be obtained directly in one. In this manner, three couplings, $^1J_{NH}$, $^1J_{NC}$, and $^2J_{CH}$, can be measured. Again, the spectra exhibit the same resolution as the above (δ, J)-E.COSY spectrum, with each cross peak shifted by the passive couplings. The sensitivity is higher than in the normal HNCO experiment. In addition, the pulse sequence in (b) can be easily extended into a 3D version, if so desired, by adding a new frequency dimension. For example, using the CO frequency would allow to further resolve peaks in crowded regions of the (δ, J)-E.COSY spectrum.

Fig. 2a displays one of the two spectra using the pulse sequence of Fig. 1b recorded on a 1 mM sample of uniformly ^{13}C, ^{15}N labeled protein GB1 with 56 amino acid residues [25] in a liquid crystalline phase of 15 mg/ml PF1 at pH $\approx$ 7. As an example, the relevant couplings and frequencies are indicated for one cross peak pair. As can be appreciated, it is straightforward to extract the couplings from the spectra. Simple peak-picking of the two spectra yields complete sets of one-bond ^{15}N–$^1H^N$ and ^{15}N–$^{13}C'$ and two-bond $^{13}C'$–$^1H^N$ couplings for GB1. The measured dipolar couplings correlate excellently with those predicted from the 1.1 Å crystal structure (PDB code: 1IGD) [26] and refined NMR structure (PDB code: 3GB1) [27]. Correlations between measured and predicted values for three types of dipolar couplings are displayed in Fig. 2b–d. Slightly better agreement between observed and predicted values is obtained when using the refined NMR structure (the linear correlation coefficients are 0.99, 0.97, and 0.92 for $^1D_{NH}$, $^2D_{HC'}$, and $^1D_{NC'}$, respectively) compared to using the 1.1 Å X-ray structure (The linear correlation coefficients are 0.98, 0.94, and 0.90 for $^1D_{NH}$, $^2D_{HC'}$, and $^1D_{NC'}$, respectively). Whether this reflects a genuine difference between solution and X-ray structures is hard to ascertain. It should be pointed out, nevertheless, that the NMR structure was refined against residual dipolar couplings [27]. These, however, were measured in liquid crystalline bicelles and TMV and as such are not identical to those obtained here. The values for the magnitude and rhombicity of the alignment tensor for the refined NMR (PDB code: 3GB1) and 1.1 Å X-ray (PDB code: 1IGD) structures are $D_a^{NH} = 6.8$ Hz and $R = 0.628$ and $D_a^{NH} = 7.0$ Hz and $R = 0.616$, respectively.

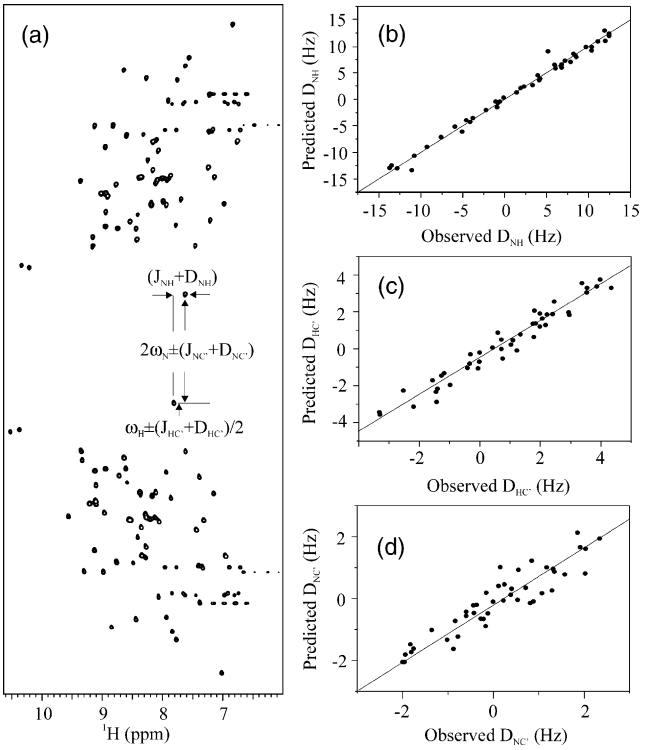

Fig. 2. (a) Experimental 2D sensitivity-enhanced (δ, J)-E.COSY HSQC recorded on a 1 mM sample of uniformly ^{13}C, ^{15}N labeled protein GB1 dissolved in liquid crystalline PF1 (15 mg/ml) in 95%H_2O/5%D_2O at pH $\approx$ 7 employing the pulse scheme presented in Fig. 1b. The spectrum was recorded on a Bruker DMX 500 spectrometer with a ^1H frequency of 500.13 MHz. The 2D spectral widths were $SW_1 \times SW_2 = 4000 \times 7507.507$ Hz; the time domain data set was $TD_1 \times TD_2 = 512 \times 1024$; ns = 32; window functions in both dimensions were squared sine bell; the data set was zero filled to 1024×1024; the recycle delay = 1 s. Data were processed by using nmrPipe and nmrDraw software [28]. (b)–(d) show the correlations between measured dipolar couplings and predicted values using the refined NMR structure (PDB code: 3GB1) [27]. Prediction was performed by SSIA [29] and the straight line represents the linear regression.

In conclusion, we demonstrated that the (δ, J)-E.COSY spectra described here are ideally suited for the measurement of residual dipolar couplings. There is no loss in resolution when compared to decoupled HSQC spectra and the sensitivity is 1.4 times that of the coupled HSQC spectra. There is no need for hetero-nuclear decoupling during data acquisition, avoiding any problems associated with heating and no time limit in real time detection exists. The digital resolution in the ω_2 dimension can be set high, within the limits imposed solely by the line-widths. The accuracy of experimentally determined couplings can be controlled by the experimental digital resolution. When compared to the popular IPAP method [10], the pulse sequence laid out in Fig. 1a for measuring one-bond ^{15}N–$^1H^N$ couplings is much simpler and the spectrum is easier to analyze. Most notably, the pulse sequence presented in Fig. 1b

for measuring one-bond ^{15}N–$^{1}H^{N}$ and ^{15}N–$^{13}C'$ and two-bond $^{13}C'$–$^{1}H^{N}$ couplings is superior to any of the existing methods. Therefore, these novel experiments are extremely valuable for measuring residual dipolar couplings in proteins.

Acknowledgments

This work was supported in part by the Intramural AIDS Targeted Antiviral Program of the Office of the Director of the National Institutes of Health to AMG.

References

[1] N. Tjandra, J.G. Omichinski, A.M. Gronenborn, G.M. Clore, A. Bax, Nature Struct. Biol. 4 (1997) 732–738.
[2] A. Bax, G. Kontaxis, N. Tjandra, Method Enzymol. 339 (2001) 127–174.
[3] E. de Alba, N. Tjandra, Prog. Nucl. Magn. Reson. Spectrosc. 40 (2002) 175–197.
[4] N. Tjandra, A. Bax, Science 278 (1997) 1111–1114.
[5] G.M. Clore, M.R. Starich, A.M. Gronenborn, J. Am. Chem. Soc. 120 (1998) 10571–10572.
[6] R. Tycko, F.J. Blanco, Y. Ishii, J. Am. Chem. Soc. 122 (2000) 9340–9341.
[7] N. Tjandra, S. Grzesiek, A. Bax, J. Am. Chem. Soc. 118 (1996) 6264–6272.
[8] J.R. Tolman, J.H. Prestegard, J. Magn. Reson. B 112 (1996) 245–252.
[9] J.R. Tolman, J.H. Prestegard, J. Magn. Reson. B 112 (1996) 269–274.
[10] M. Ottiger, F. Delaglio, A. Bax, J. Magn. Reson. 131 (1998) 373–378.
[11] A. Bax, G.W. Vuister, S. Grzesiek, F. Delaglio, A.C. Wang, R. Tschudin, G. Zhu, Method Enzymol. 239 (1994) 79–105.
[12] J.J. Chou, F. Delaglio, A. Bax, J. Biomol. NMR 18 (2000) 101–105.
[13] C. Griesinger, O.W. Sorensen, R.R. Ernst, J. Am. Chem. Soc. 107 (1985) 6394–6396.
[14] M. Ottiger, A. Bax, J. Am. Chem. Soc. 120 (1998) 12334–12341.
[15] D. Neuhaus, G. Wagner, M. Vasak, J.H.R. Kaegi, K. Wüthrich, Eur. J. Biochem. 151 (1985) 257.
[16] O.W. Sørensen, G.W. Eich, M.H. Levitt, G. Bodenhausen, R.R. Ernst, Prog. Nucl. Magn. Reson. Spectrosc. 16 (1983) 163–192.
[17] A.G. Palmer III, J. Cavanagh, P.E. Wright, M. Rance, J. Magn. Reson. 93 (1991) 151–170.
[18] J. Cavanagh, A.G. Palmer III, P.E. Wright, M. Rance, J. Magn. Reson. 91 (1991) 429–436.
[19] K. Ding, A.M. Gronenborn, J. Magn. Reson. 156 (2002) 262–268.
[20] G. Drobny, A. Pines, S. Sinton, D. Weitekamp, D. Wemmer, Faraday Div. Chem. Soc. Symp. 13 (1979) 49.
[21] G. Bodenhausen, R.L. Vold, R.R. Vold, J. Magn. Reson. 37 (1980) 93–106.
[22] D. Moskau, Concepts Magn. Reson. 15 (2002) 164–176.
[23] J.J. Chou, S. Li, C.B. Klee, A. Bax, Nature Struct. Biol. 8 (2001) 990–997.
[24] D.J. States, R.A. Haberkorn, D.J. Ruben, J. Magn. Reson. 48 (1982) 286–292.
[25] A.M. Gronenborn, D.R. Filpula, N.Z. Essig, A. Achari, M. Whitlow, P.T. Wingfield, G.M. Clore, Science 253 (1991) 657–661.
[26] J.P. Derick, D.B. Wigley, J. Mol. Biol. 243 (1994) 906–918.
[27] J. Kuszewski, A.M. Gronenborn, G.M. Clore, J. Am. Chem. Soc. 121 (1999) 2337–2338.
[28] F. Delaglio, S. Grzesiek, G.W. Vuister, G. Zhu, J. Pferfer, A. Bax, J. Biomol. NMR 6 (1995) 277–293.
[29] M. Zweckstetter, A. Bax, J. Am. Chem. Soc. 122 (2000) 3791–3792.